

Investigation of structural and some physical properties of Cr substituted polycrystalline $\text{Eu}_{0.5}\text{Sr}_{0.5}\text{Mn}_{1-x}\text{Cr}_x\text{O}_3$ ($0 \leq x \leq 0.1$) manganites

Anchit Modi¹ · Masroor Ahmad Bhat¹ · Shovit Bhattacharya² · N. K. Gaur¹

Received: 14 February 2016 / Accepted: 25 April 2016 / Published online: 29 April 2016
© Springer Science+Business Media New York 2016

Abstract The polycrystalline samples with nominal composition $\text{Eu}_{0.5}\text{Sr}_{0.5}\text{Mn}_{1-x}\text{Cr}_x\text{O}_3$ ($0 \leq x \leq 0.1$) were prepared by the conventional solid state reaction method and characterized by X-ray diffraction, scanning electron microscopy and electrical resistivity behavior without and with magnetic field. The structural parameters obtained by using Rietveld refinement of X-ray diffraction data showed that all samples crystallize with orthorhombic perovskite type symmetry with $Pbnm$ space group. The scanning electron micrograph images reveal that the increase in Cr substitution hinders grain growth and grain connectivity. The temperature dependence of electrical resistivity show the semiconducting nature of these compounds and support the small polaron hopping model and variable range hopping conduction model. The calculated hopping distance and activation energy decreased as rate of Cr content increased whereas density of states at Fermi level increased. A large negative magnetoresistance is also present in the sample at the lowest temperature of measurements.

1 Introduction

In the recent years, the perovskite manganites with a general formula $\text{Ln}_{1-x}\text{B}_x\text{MnO}_3$ (Ln is a trivalent rare earth cation and B is bivalent alkaline earth cation) have engrossed wide research interest, due to their remarkable

magnetic and transport properties, especially the colossal magneto-resistance and electro-resistance phenomenon demonstrated by them and rich physics behind their novel phase diagrams leading to potential application in magnetic, magneto-electronic, photonic devices, infrared detector, as well as spintronics technology [1–6]. Zener's double exchange (DE) interaction between Mn^{3+} and Mn^{4+} ions through charge carriers in the oxygen 2p orbital's was introduced in order to explain the magnetic and electric properties in these compounds [7]. However, several studies clearly indicated that various factors such as mixed valency, ionic size mismatch, Mn–O bond lengths, Mn–O–Mn bond angles, oxygen stoichiometry, Jahn–Teller (JT) distortion and grain boundary effect play an important role in electrical and magnetic properties of manganites [8–10].

The charge ordered phase in manganites with the perovskite structure of the half doped $\text{R}_{0.5}\text{A}_{0.5}\text{MnO}_3$ demonstrates a variety of exciting physical phenomenon such as charge, orbital and spin ordering the magnetic field and current driven transitions. The competition between AFM and FM interaction in very strong around ($x \approx 0.5$) and ground state magnetic nature can easily be influenced by external applied magnetic field [11–14]. Among mixed-valent manganites, $\text{Eu}_{1-x}\text{Sr}_x\text{MnO}_3$ compounds is one of the well studied systems which show AFM ground state owing to smaller Eu^{3+} ions [15]. Dutta et al. [16] reported that the charge ordered manganites $\text{Eu}_{0.5}\text{Sr}_{0.5}\text{MnO}_3$ shows PM to AFM transition on cooling, which results insulating behavior of the compound down to the lowest temperature of measurement and on application of H, the AFM insulation state transforms to a metallic FM state showing first-order IM transition on cooling. Cao et al. [14] said that the substitution on Mn site are found to be an effective way to modify the charge/orbital-ordered (CO/OO) and antiferromagnetic

✉ Anchit Modi
anchitmodi87@gmail.com

¹ Superconductivity Research Lab, Department of Physics, Barkatullah University, Bhopal 462026, India

² Technical Physics Division, Bhabha Atomic Research Center, Mumbai 400085, India

insulating phase gradually with changing of both temperature and applied magnetic field. In order to get further understanding of this mechanism, Mn substitution by various ions such as transition metals Cr has been extensively studied. The choice of Cr^{3+} is based on the fact that its electronic structure is the same as that of Mn^{4+} . Its ionic radius (0.615 Å) is smaller than the one of Mn^{3+} (0.645 Å) [17]. Some authors have proposed that Cr may participate in the double exchange (DE) interaction [18]. Modi et al. [19] suggest that there exists a poor DE interaction between Mn^{3+} and Cr^{3+} at high temperature so that Cr^{3+} can not play the role of Mn^{4+} in the $\text{Mn}^{3+}\text{--O--Cr}^{3+}$ interaction. Correspondingly, Cr^{3+} partially plays the role of Mn^{4+} in the low temperature range. However, other authors argued that $\text{Mn}^{3+}\text{--O--Cr}^{3+}$ exchange interaction is super-exchange rather than DE. It is reported that Chromium is the most efficient one to induce a metal insulator transition in the CO manganites and leads to a much higher CMR effect [14]. In the present work, we have undertaken the study of Cr substituted $\text{Eu}_{0.5}\text{Sr}_{0.5}\text{Mn}_{1-x}\text{Cr}_x\text{O}_3$ synthesized by mixed oxide reaction and the crystallographic structure, microstructure and magnetotransport properties were systematically investigated.

2 Experimental procedure

The polycrystalline samples $\text{Eu}_{0.5}\text{Sr}_{0.5}\text{Mn}_{1-x}\text{Cr}_x\text{O}_3$ ($0 \leq x \leq 0.1$) were synthesized by conventional solid-state reaction technique from high purity ($\leq 99.99\%$ Aldrich) stoichiometric quantities of Eu_2O_3 (Preheated at 500 °C for 6 h), MnO_2 and Cr_2O_3 . The powders were mixed and thoroughly grinded for 8–10 h in an agate pestle mortar and the slurry calcined at 1150 °C for 24 h in air. This process were repeated several times until single-phase sample obtained and the resulting powders were the subsequently pulverized, and compressed it into pellets of 10 mm diameters and approximately 1–2 mm thickness under a hydraulic pressure of 8–10 tons. The pellets were sintered at 1250 °C for 24 h in order to get complete reaction and required compactness. All samples were slowly cool down to room temperature to maximize the oxygen content.

The X-ray diffraction pattern (XRD) for all the samples were examined by using Bruker D8 Advance diffractometer with $\text{Cu K}\alpha_1$ ($\lambda = 1.5406 \text{ \AA}$) radiation operating at 40 kV/100 mA. The data collected from 20° to 80° in 2 θ range with steps size 0.02° and a counting time 15 s/steps. The XRD data were refined by means of the Rietveld refinement technique using FULLPROF program to confirm the phase formation as well as to obtain the lattice parameters, space group and crystal system. The surface morphological analysis of the samples was investigated by

scanning electron microscopy (SEM) at room temperature on a JSM-6400 apparatus working at 20 kV. The electrical resistivity measurements were carried out by standard four-probe method in the temperature range 5–300 K at 0 and 8 T magnetic field. Electrical contacts were made by indium on a rectangular rod of the sample.

3 Results and discussion

3.1 Structural and microstructural properties

The powder XRD patterns of $\text{Eu}_{0.5}\text{Sr}_{0.5}\text{Mn}_{1-x}\text{Cr}_x\text{O}_3$ ($0 \leq x \leq 0.1$) compounds at room temperature and the corresponding fit using Rietveld refinements for all the samples are shown in Fig. 1. The data are fitted over 2 θ range 20°–80°, which reveal that all the samples are single phased with no detectable impurity within the experimental limits. Further the sharp peaks indicate that the samples are highly crystalline. All the samples in the present investigation are indexed shows the class of orthorhombic perovskite structure having *Pbnm* space group. In this refinement, the whycoff atomic positions are considered as follows: (Eu, Sr) atoms are at 4c (x, y, 1/4) positions, Mn at 4b (1/2, 0, 0) and O_1 at 4c (x, y, 1/4) and O_2 at 8d (x, y, z) position. The profile refinement was started with scale and background parameters followed by unit cell parameters.

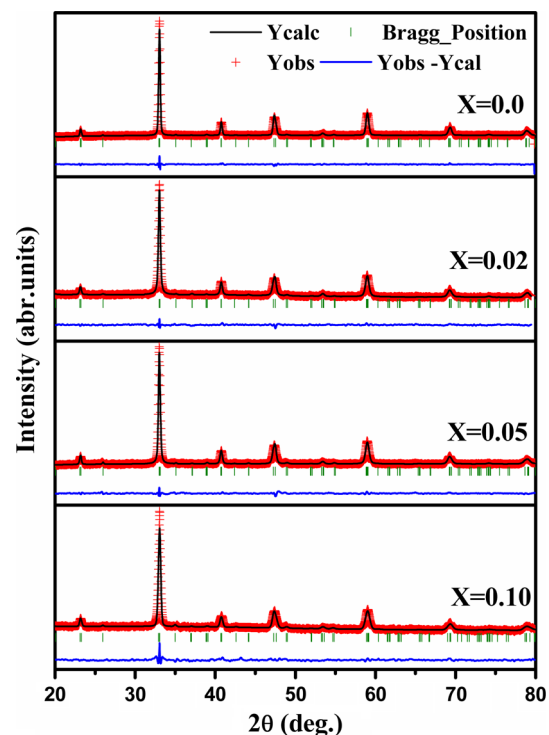


Fig. 1 Rietveld fitted XRD pattern of $\text{Eu}_{0.5}\text{Sr}_{0.5}\text{Mn}_{1-x}\text{Cr}_x\text{O}_3$ ($0 \leq x \leq 0.1$) compounds at 300 K

Then, the peak asymmetry and preferred orientation correction are applied. Finally, the position parameter and individual isotropic parameters are refined. We noticed from Fig. 1 that calculated diffraction patterns match well with measured ones. The difference observed between the intensities of the measured and calculated diffraction lines can be attributed by the existence of preferential orientation of the crystallites in the samples. Positions for the Bragg reflection are marked by vertical bars. Differences between the observed and the calculated intensities are shown at the bottom of the diagram. The lattice parameters, the atomic positions, and other relevant parameters of interest are summarized in Table 1. It is noticed that with increasing Cr content, a decrease in cell volume is observed. This is

Table 1 Rietveld refined structural parameters of $\text{Eu}_{0.5}\text{Sr}_{0.5}\text{Mn}_{1-x}\text{Cr}_x\text{O}_3$ ($0 \leq x \leq 0.1$) samples

Composition (x)	X = 0	X = 0.02	X = 0.05	X = 0.1
<i>Space group</i>	<i>Pbnm</i>	<i>Pbnm</i>	<i>Pbnm</i>	<i>Pbnm</i>
<i>Lattice parameter</i>				
a(Å)	5.4286(15)	5.4075(19)	5.4045(10)	5.4038(3)
b(Å)	5.4249(16)	5.4201(17)	5.4181(12)	5.4104(3)
c(Å)	7.6419(7)	7.6377(12)	7.6378(10)	7.6360(2)
V(Å) ³	225.050	223.854	223.650	223.215
<i>Positional parameter</i>				
Eu/Sr: x	0.001(4)	0.011(2)	0.007(3)	0.004(3)
y	0.0161(12)	0.006(2)	0.0216(9)	0.0218(6)
z	1/4	1/4	1/4	1/4
Mn/Cr: x	1/2	1/2	1/2	1/2
O1: x	0.076(9)	0.004(4)	0.569(12)	0.398(17)
y	0.500(8)	0.596(7)	0.995(6)	1.022(11)
z	1/4	1/4	1/4	1/4
O2: x	0.773(5)	1.231(6)	0.765(8)	0.791(7)
y	0.23(3)	0.328(3)	0.184(6)	0.265(8)
z	0.013(7)	0.011(10)	0.012(8)	0.049(6)
<i>Reliability factors</i>				
R _p	37.1	59.5	48.3	54.4
R _{wp}	20.9	29.9	27.3	29.8
R _{exp}	19.42	25.83	20.72	28.01
R _{Bragg}	4.73	8.25	13.8	8.24
R _F	9.49	18.0	21.7	13.8
χ ²	1.31	1.45	1.84	1.26
<i>Bond distance (Å)</i>				
Mn-O1	1.9755(10)	2.0155(24)	1.9528(12)	1.9145(58)
Mn-O2	1.9694(10)	2.1984(18)	2.0449(54)	1.9042(96)
Mn-O3	1.8929(21)	1.6655(10)	1.8731(59)	2.0673(87)
<i>Bondangles (degree)</i>				
Mn-O1-Mn	155.3(4)	142.7(10)	155.8(5)	171.3(3)
Mn-O2-Mn	167.2(9)	167(5)	157(2)	150(4)

possibly because of the replacement of relatively larger Mn³⁺ (0.64 Å) ion by the Cr³⁺ (0.62 Å) ions [20]. The possibility of replacement of Mn⁴⁺ ions by the Cr³⁺ ions is ruled out as the difference between their ionic radii is almost 0.9 Å. From the results of the average distances of Mn–O and the average angles of Mn–O–Mn, it is considered that each MnO₆ octahedron has little distortion. Further, the structural stability of the perovskite structure is determined the Goldschmidt tolerance factor $t = (r_A + r_o) / \sqrt{2}(r_B + r_o)$ which satisfy the condition for stable perovskite phase which is often found less than one.

The direct evidence of the microstructure of Cr doped sintered pellets as revealed through scanning electron microscopy images are displayed in Fig. 2. The variation of Cr composition had prominent effect on the grain morphology of the system. The samples show strongly connected large grains, forming almost homogenous particles up to a certain doping level which suggest the good crystalline quality of these compounds. It is also clear evident that grain get agglomerated and become dense on the increment of doping content. On inspection, it can be seen that grain size has improved dramatically with reduction in porosity on increasing chromium content up to x = 0.05 beyond which it separates and enhances the semiconducting mechanism. Each sample is having a grain size of 5 μm. Thus, Cr acts as a catalyst and plays a vital role on electronic and magneto-transport properties of the system.

3.2 Resistivity and conduction mechanism

Figure 3a–d illustrates the temperature dependent electrical resistivity curves in the temperature range of 5–300 K for the $\text{Eu}_{0.5}\text{Sr}_{0.5}\text{Mn}_{1-x}\text{Cr}_x\text{O}_3$ ($0 \leq x \leq 0.1$) series in the presence and absence of the magnetic field. Using the symbol of the temperature coefficient of resistivity $d\rho/dT$ as a criterion ($d\rho/dT < 0$ for an insulating/semiconductor-like and $d\rho/dT > 0$ for a metallic system), all the samples are found to be semiconductor-like character. When we substitute chromium (Cr) at Mn site give an increment in resistivity observed, it's gradually increases down to the lowest temperature of measurement and go beyond the instrumental limit. At room temperature resistivity of all compound are approximately few Ω cm range, whereas with decrease of temperature it increases rapidly and go beyond the instrumental limit. But in the presence of magnetic field (H = 8 T), compounds initiate to convert metallic behavior below the certain temperature and show the clear metal to insulator transition around 140 K is observed for X = 0 and 0.02 composition. However no such IM transition is observed in X = 0.05 and 0.1 compositions. It means that applied 8 T magnetic field is not

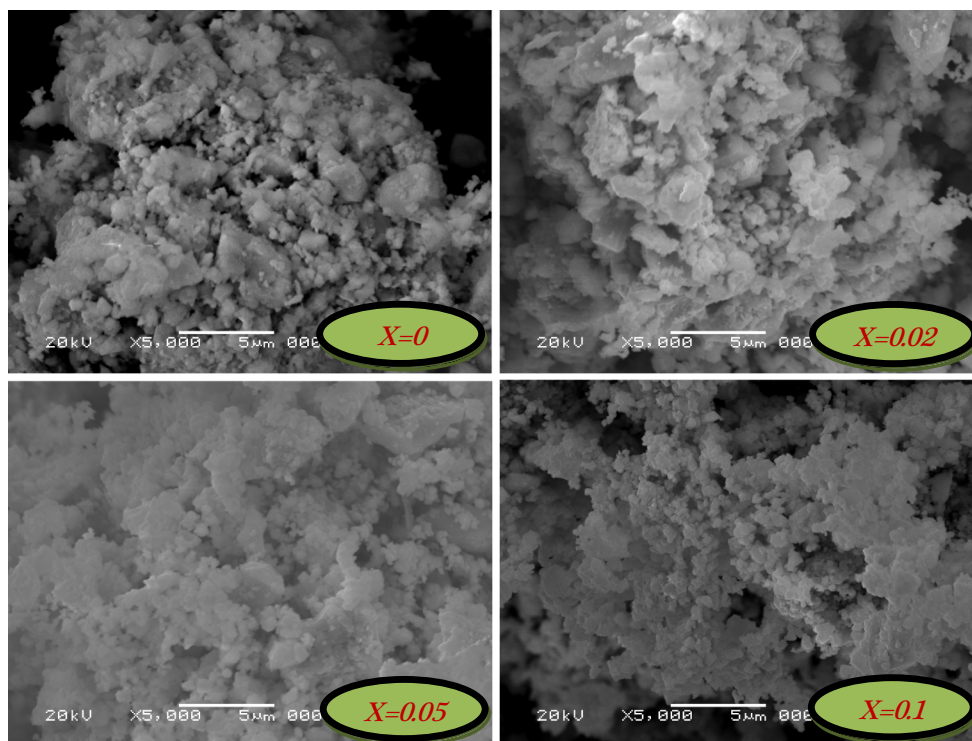


Fig. 2 Scanning electron microscope (SEM) images of $\text{Eu}_{0.5}\text{Sr}_{0.5}\text{Mn}_{1-x}\text{Cr}_x\text{O}_3$ ($0 \leq x \leq 0.1$) compounds

enough to induce metal to insulator transition for higher Cr substituted compositions. In the application of magnetic field the ferromagnetic (FM) clusters begin to develop in otherwise AFM ground state of these materials. Under the application of magnetic field, the orientation of casual ferromagnetic clusters is forced to line up homogeneously so that the degree of magnetic disorder is condensed which favor the electron delocalization and as a result results in distinct drop of resistivity which is excellent match with previous report [21].

To understand the semiconducting nature of these compounds, further resistivity data were analyzed using small polaron hopping (SPH) model and other with Mott variable range hopping (VRH). The VRH model originally verified in the lightly doped semiconductors with impurities randomly distributed. The expression for Mott-VRH model [22] is given here.

$$\rho = \rho_0 \exp\left(\frac{T^*}{T}\right)^{1/4} \quad (1)$$

With

$$k_B T^* = \frac{24}{\pi N(E_F) \xi^3} \quad (2)$$

where ρ_0 is the residual resistivity, T^* is the Mott characteristic temperature which can be expressed in the terms of the resistivity the density of states near the Fermi level is

known as $N(E_F)$ is, k_B is the Boltzmann constant and ξ is the localization length.

The most probable hopping distance R_h (T) and the hopping energy W_h (T) can be written [23, 24] at a given temperature T, as

$$R_h(T) = \frac{3}{8} \xi \left(\frac{T^*}{T}\right)^{1/4} \quad (3)$$

$$W_h(T) = \frac{1}{4} k_B T^{3/4} (T^*)^{1/4} \quad (4)$$

The $\ln(\rho)$ versus $(1/T)^{-1/4}$ plot in Fig. 4a, b shows the linear behavior and fitted data which are shown as solid line. Using the fitted values of T^* obtained from the above equations, we have estimated the values of $N(E_F)$, R_h and W_h by taking the localization length ξ ($c =$ lattice parameter from Table 1) and listed in Table 2. It is clearly noticed that from Table 2, with increasing the Cr doping concentration the density of states at Fermi level $N(E_F)$ increases from $9.606 \times 10^{19} \text{ eV}^{-1} \text{ cm}^{-3}$ for $X = 0$ to $17.8148 \times 10^{19} \text{ eV}^{-1} \text{ cm}^{-3}$ for $X = 0.1$ whereas value of T^* decreased from $8.473 \times 10^6 \text{ K}$ in the case of $X = 0$ and $4.6185 \times 10^6 \text{ K}$ for $X = 0.1$ compound. We also estimated the hopping length and hopping energy in decreasing trend with the increasing rate of Cr concentration. These observations are consistent with the earlier report which suggested that as long as the members of this series are in semiconducting region, they obey VRH model over a limited range of temperature [25].

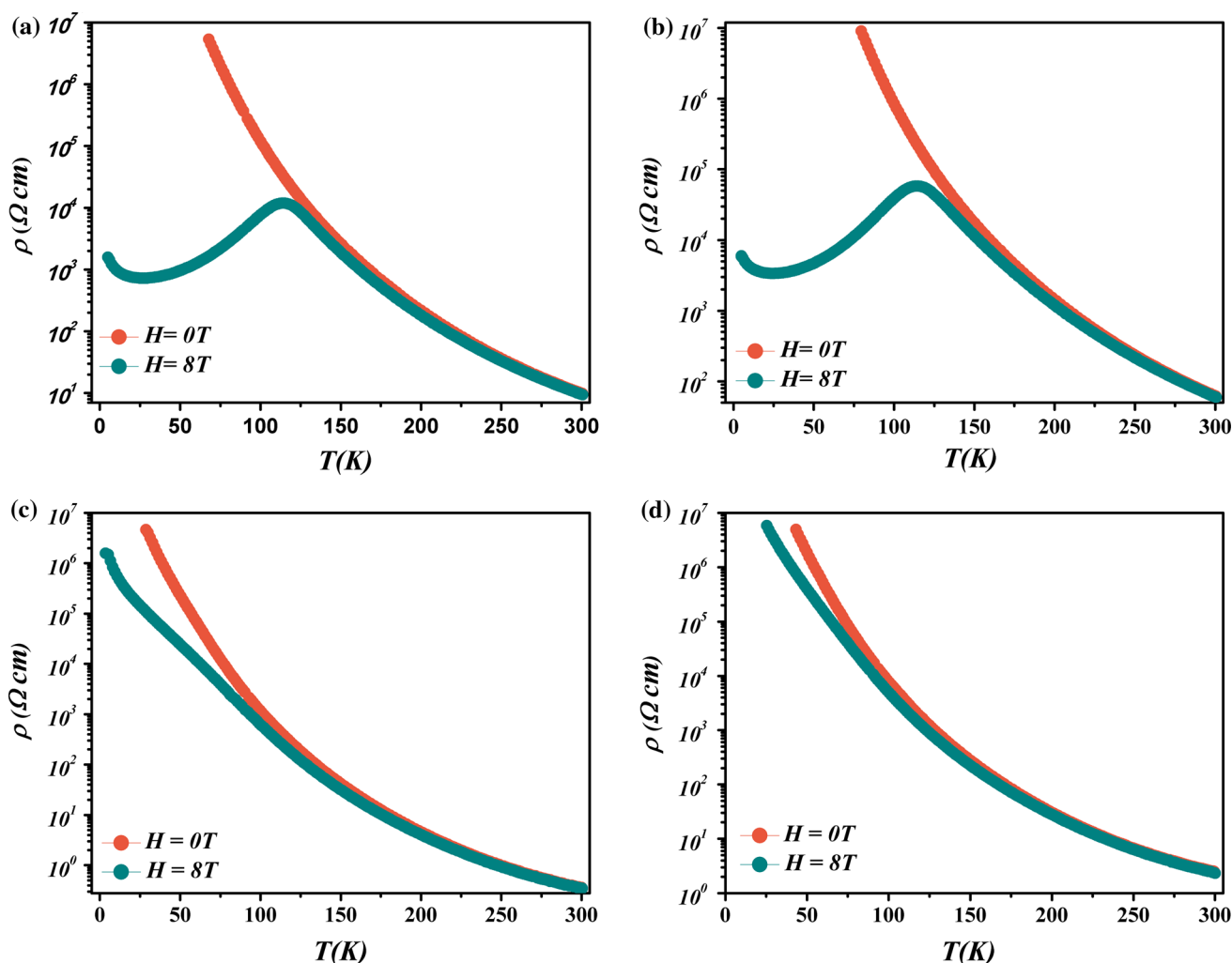


Fig. 3 Temperature dependence of electrical resistivity of $\text{Eu}_{0.5}\text{Sr}_{0.5}\text{Mn}_{1-x}\text{Cr}_x\text{O}_3$ ($0 \leq x \leq 0.1$) compounds in the presence of 0 and 8 T applied magnetic field **a** for $X = 0$, **b** for $X = 0.02$, **c** for $X = 0.05$ and **d** for $X = 0.1$ respectively

The origin of the small polarons in manganites is the Jahn–Teller distortion due to the presence of Mn^{3+} ions in these system which results in the possibility of strong electron–phonon coupling and hence self-localization of the charge carriers [26]. In order to gain the better insights into the nature of interaction between the hopping conduction and the strength of electron–phonon interaction, the temperature dependence of resistivity data have been fitted the small polaron hopping model [27] is given as

$$\rho/T = \rho_z \exp(E_p/k_B T), \tag{5}$$

where $\rho_z = [k_B/v_{ph}Ne^2R^2C(1 - C)] \exp(2\alpha R)$, k_B is the Boltzmann constant, and T is the absolute temperature. N is the number of ion sites per unit volume, R is the average intersite spacing obtain from the relation $R = (1/N)^{1/3}$, C is the fraction of site occupied by the polaron, α is the electron wave function decay constant and E_p is the activation energy. The polaron activation energy can be estimated

form slope of the resistivity curve as $\ln(\rho)$ versus $1/T$ curve displayed in Fig. 4c, d and calculated activation energy E_a tabulated in Table 2. Both the models described our result in the semiconducting phase fairly well and give the best correlation factor R .

3.3 Magnetoresistance

The change in resistance under magnetic field in termed as magetoresistance (MR) and its variation with temperature is derived by using following relation such as

$$MR\% = \frac{\rho(H) - \rho(0)}{\rho(0)} \times 100 \tag{6}$$

where $\rho(H)$ and $\rho(0)$ are the high field and zero field resistivity respectively. The measured MR is shown in inset of Fig. 5 for all the reported compounds. It is clearly observed that all the compounds show the negative MR

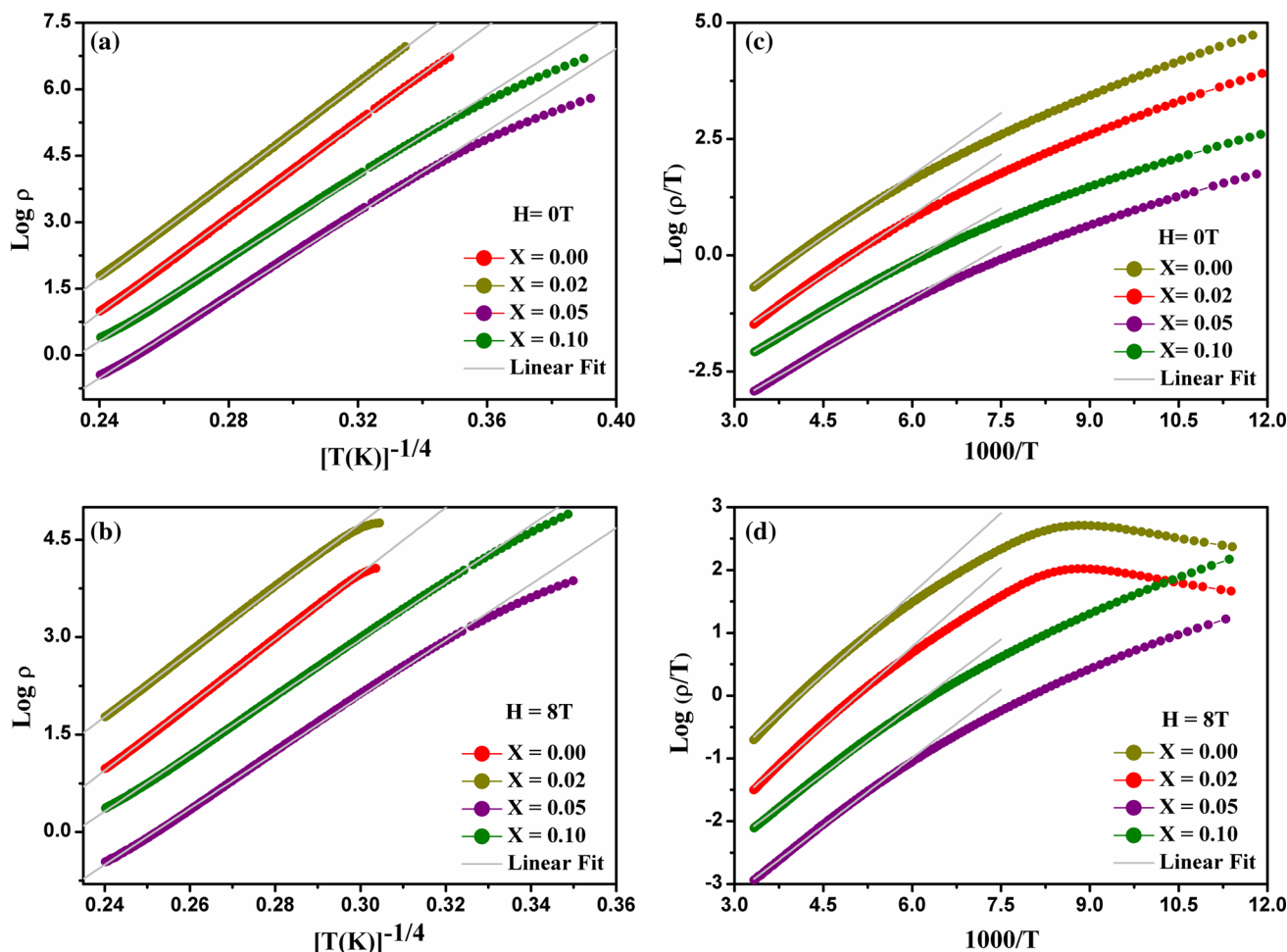


Fig. 4 The plot $\text{Log}(\rho)$ versus $(1/T)^{-1/4}$ for $\text{Eu}_{0.5}\text{Sr}_{0.5}\text{Mn}_{1-x}\text{Cr}_x\text{O}_3$ ($0 \leq x \leq 0.1$) compounds in **a** and **b** panel at 0 and 8 T applied magnetic field respectively. The relation between $\text{Log}(\rho/T)$ versus

$1000/T$ for $\text{Eu}_{0.5}\text{Sr}_{0.5}\text{Mn}_{1-x}\text{Cr}_x\text{O}_3$ ($0 \leq x \leq 0.1$) compounds in **c** and **d** panel at 0 and 8 T applied magnetic field respectively

Table 2 The fitted parameters to the experimental resistivity data of $\text{Eu}_{0.5}\text{Sr}_{0.5}\text{Mn}_{1-x}\text{Cr}_x\text{O}_3$ ($0 \leq x \leq 0.1$) using VRH and SPH Models

Compositions/parameters	X = 0		X = 0.02		X = 0.05		X = 0.1	
	0 T	8 T	0 T	8 T	0 T	8 T	0 T	8 T
$T^* (\times 10^6 \text{K})$	9.055	6.561	8.474	6.102	4.918	3.847	4.618	3.769
$N(E_F) \times 10^{19} (\text{eV}^{-1} \text{cm}^{-3})$	8.990	12.40	9.607	13.34	16.55	21.16	17.625	21.59
$R_h (\text{\AA})$	10.97	10.12	10.79	9.941	9.420	8.859	9.273	8.814
$W_h (\text{meV})$	85.15	78.56	83.75	77.15	73.10	68.74	71.96	68.40
$E_a (\text{meV})$ SPH	74.25	74.04	73.61	72.93	63.01	61.60	61.89	61.17

over the measurement range. The magnitude of MR increases with decreasing temperature and found to be maximum at the lowest temperature of measurement. MR is recorded to be more than -99.9% in presence of 8 T magnetic field around 40 K for $X = 0$ and 0.02 sample. Whereas, for $X = 0.05$ and 0.1 samples MR is about -89 and -78% respectively at 40 K. Melting of AFM clusters into the FM state results this large negative MR, as commonly observed in CMR manganites very good match with

previous report [16]. The parent compound $\text{Eu}_{0.5}\text{Sr}_{0.5}\text{MnO}_3$ illustrates a much higher MR value than the Cr substituted compounds. It is thought that the 8 T magnetic field is too low to destroy the charge ordering phase completely, a higher magnetic field it needed to orient magnetic domains and induced the formation of FM state, thus cause a relatively higher value of MR for the parent compound the similar phenomena is observed in another charged ordered manganites $\text{Pa}_{0.5}\text{Ca}_{0.5}\text{MnO}_3$ [14]. However, the increment

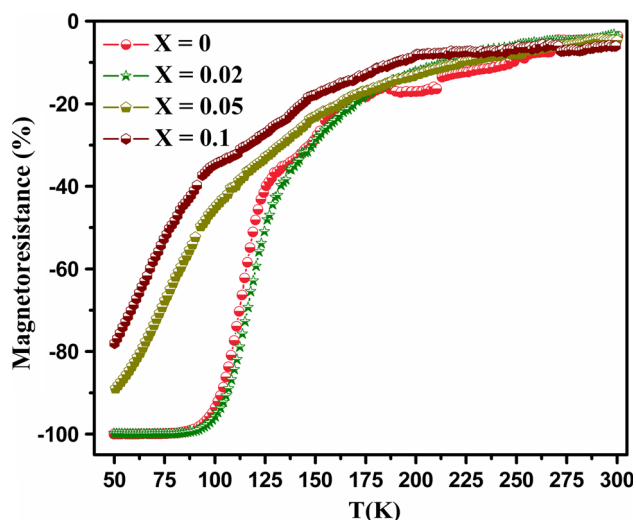


Fig. 5 Temperature dependence of MR for the compounds of $\text{Eu}_{0.5}\text{Sr}_{0.5}\text{Mn}_{1-x}\text{Cr}_x\text{O}_3$ ($0 \leq x \leq 0.1$) at 8 T

of Cr concentration gradually suppressed the charged ordering phase, including the formation of ferromagnetic cluster responsible to decrease the MR value. A ferromagnetic matrix containing anti-ferromagnetic clusters should give rise to a remarkable magnetoresistance effects as observed in the samples. Therefore, the MR effect of the reported system is believed to mainly result from the melting of the charge ordered phase and the phase separation caused by the Cr doping and the mechanism of the MR effect is different for the undoped samples.

4 Conclusion

In summary, structural and magnetotransport properties of the polycrystalline $\text{Eu}_{0.5}\text{Sr}_{0.5}\text{Mn}_{1-x}\text{Cr}_x\text{O}_3$ ($0 \leq x \leq 0.1$) perovskites synthesized by solid state reaction method have been studied systematically. The structure study shows that all our synthesized compounds crystallize in the orthorhombic structural with *Pbnm* space group. The lattice parameters and unit cell volume decrease with increasing the Cr concentration. This might be due to the smaller size of ionic radii of Cr^{3+} as compared to Mn^{3+} ions. The magnetoresistance increases with decreasing temperature and it reach maximum at the lowest temperature. It is observed -99.9% for parent compound as well as small Cr doped compound whereas for higher doping it suppress. Resistivity behavior fits well for all the samples with the VRH model and SPH model for the measured temperatures range signifying that the conduction mechanism. However, with the increasing rate of Cr substitution and applied magnetic field, the density of states at Fermi level increases

while hopping length, hopping energy and activation energy decreases, which suggest that the Cr doping at Mn site, enhance the ferromagnetic coupling.

Acknowledgments The authors are thankful to University Grant Commission (UGC), New Delhi for providing the financial support. Authors are thankful to UGC-DAE CSR, Indore for providing characterization facilities. Authors are gratefully acknowledged Dr. Rajeev Rawat and Dr. Mukul Gupta for fruitful discussion.

References

1. S. Jin, T.H. Tiefel, M. Mc Cormack, R.A. Fastnacht, R. Ramesh, L.H. Chen, *Science* **254**, 413 (1994)
2. Z.B. Guo, Y.W. Du, J.S. Zhu, H. Huang, W.P. Ding, D. Feng, *Phys. Rev. Lett.* **78**, 1142 (1997)
3. A. Urushibara, Y. Moritomo, T. Arima, A. Asamitsu, G. Kido, Y. Tokura, *Phys. Rev. B* **51**, 14103 (1995)
4. T.S. Orlova, J.Y. Laval, P. Monod, P. Bassoul, J.G. Noudem, E.V. Orlenko, *Phys. Rev. B* **79**, 134407 (2009)
5. R. Bellouz, M. Oumezzine, A. Dinia, G. Schmerber, E.L.K. Hlil, M. Oumezzine, *RSC Adv.* **5**, 64557 (2015)
6. Y. Sun, W. Tong, X. Xu, Y. Zhang, *Phys. Rev. B* **63**, 174438 (2001)
7. C. Zener, *Phys. Rev. B* **82**, 403 (1951)
8. A.J. Millis, *Phys. Rev. B* **53**, 8434 (1996)
9. P.K. Siwach, H.K. Singh, O.N. Srivastava, *J. Phys. Condens. Matter* **20**, 273201 (2008)
10. M.A. Bhat, A. Modi, N.K. Gaur, *J. Mater. Sci. Mater. Electron.* **26**, 6444 (2015)
11. C. Autret, A. Maigna, C. Martin, M. Hervieu, V. Hardy, S. Hebert, B. Reveau, *Appl. Phys. Lett.* **82**, 4746 (2003)
12. R.J. Goff, J.P. Attfield, *Phys. Rev. B* **70**, 140404(R) (2004)
13. S. Mori, R. Shoji, N. Yamamoto, T. Asaka, Y. Matsui, A. Machida, Y. Moritomo, T. Katsufuji, *Phys. Rev. B* **67**, 012403 (2003)
14. S. Cao, W. Li, J. Zhang, B. Kang, T. Gao, C. Jing, *J. Appl. Phys.* **102**, 053909 (2007)
15. Y. Tomioka, R. Kumai, T. Ito, Y. Tokura, *Phys. Rev. B* **80**, 174414 (2009)
16. P. Dutta, D. Das, S. Chatterjee, S. Majumdar, *J. Alloys Compd.* **590**, 313 (2014)
17. N. Kumar, H. Kishan, Ashok Rao, V.P.S. Awana, *J. Appl. Phys.* **107**, 083905 (2010)
18. F.C. Fonseca, A.S. Carneiro, R.F. Jardim, J.R. O'Brien, T. Kimura, *J. Appl. Phys.* **95**, 7085 (2004)
19. A. Modi, N.K. Gaur, *J. Alloys Compd.* **644**, 575 (2015)
20. R.D. Shannon, *Acta Crystallogr. A* **32**, 751 (1976)
21. D.-Q. Liao, Y. Sun, R.-F. Yang, Z.-H. Cheng, *Phys. B* **394**, 104 (2007)
22. J.M.D. Cowy, M. Viret, S. Von Molnar, *Adv. Phys.* **48**, 167 (1999)
23. W. Khan, A.H. Naqvi, M. Gupta, S. Husain, R. Kumar, *J. Chem. Phys.* **135**, 054501 (2011)
24. S.K. Srivastava, S. Ravi, *J. Super. Nov. Magn.* **22**, 651658 (2009)
25. W.H. Jung, *J. Mater. Sci. Lett.* **17**, 1317 (1998)
26. M.W. Shaikh, I. Mansuri, M.A. Dar, D. Varshney, *Mat. Sci. Semicon. Proc.* **35**, 10 (2015)
27. A.S. Alexandrov, B.Y. Yavidov, *Phys. Rev. B* **69**, 073101 (2004)